

# SPIDER: Scalable Physics-Informed Dexterous Retargeting

Chaoyi Pan<sup>1,2,\*</sup>, Changhao Wang<sup>1</sup>, Haozhi Qi<sup>1</sup>, Zixi Liu<sup>1</sup>, Homanga Bharadhwaj<sup>1</sup>, Akash Sharma<sup>1</sup>, Tingfan Wu<sup>1,†</sup>, Guanya Shi<sup>2,†</sup>, Jitendra Malik<sup>1,†</sup>, Francois Hogan<sup>1,†</sup>

<sup>1</sup>FAIR at Meta, <sup>2</sup>Carnegie Mellon University

\*Work done at Meta, <sup>†</sup>Joint last author

Learning dexterous and agile policy for humanoid and dexterous hand control requires large-scale demonstrations, but collecting robot-specific data is prohibitively expensive. In contrast, abundant human motion data is readily available from motion capture, videos, and virtual reality, which could help address the data scarcity problem. However, due to the embodiment gap and missing dynamic information like force and torque, these demonstrations cannot be directly executed on robots. To bridge this gap, we propose Scalable Physics-Informed DExterous Retargeting (SPIDER), a physics-based retargeting framework to transform and augment kinematic-only human demonstrations to dynamically feasible robot trajectories at scale. Our key insight is that human demonstrations should provide global task structure and objective, while *large-scale physics-based sampling* with *curriculum-style virtual contact guidance* should refine trajectories to ensure dynamical feasibility and correct contact sequences. **SPIDER** scales across diverse 9 humanoid/dexterous hand embodiments and 6 datasets, improving success rates by 18% compared to standard sampling, while being 10× faster than reinforcement learning (RL) baselines, and enabling the generation of a 2.4M frames dynamic-feasible robot dataset for policy learning. As a universal physics-based retargeting method, **SPIDER** can work with diverse quality data and generate diverse and high-quality data to enable efficient policy learning with methods like RL.

**Date:** February 9, 2026

**Correspondence:** [chaoyip@andrew.cmu.edu](mailto:chaoyip@andrew.cmu.edu)

**Website:** <https://jc-bao.github.io/spider-project>



## 1 Introduction

Table-top manipulation has rapidly advanced by learning from massive internet-scale datasets (Kim et al., 2024; Khazatsky et al., 2024; Brohan et al., 2023) and human demonstrations (Team, 2025; Qu et al., 2025). Yet, acquiring generalizable whole-body manipulation across embodiments, from dexterous hands (Yin et al., 2025b; Zhong et al., 2025; Qi et al., 2023) to humanoid whole-body control (Li et al., 2025b; Ze et al., 2025), remains prohibitively expensive due to hardware constraints, task complexity, and lack of large-scale embodiment-specific data (Zhang et al., 2025; Xu et al., 2025). On the other hand, abundant human motion data is readily available, including large-scale motion-capture datasets (Zhan et al., 2024; Mahmood et al., 2019), internet-scale video collections (Ren et al., 2025), and VR-based interfaces (Hoque et al., 2025). Recent advances in computer vision have made it possible to reconstruct 3D human body (Goel et al., 2023) and hand motion (Pavlakos et al., 2024), as well as object meshes (Xiang et al., 2025) and trajectories (Wen et al., 2024), directly from videos. These developments create a unique opportunity to leverage human motion as a scalable source of demonstrations for learning humanoid and dexterous robot control. However, a fundamental challenge arises: the *embodiment gap* - the mismatch in morphology, dynamics, and actuation between humans and robots - which leads to infeasible motion during transfer. This motivates our central research question:

How can we efficiently and reliably transform human motion into feasible robot trajectories that respect dynamics and contact?

We formulate this as a physics-based retargeting problem (Reda et al., 2023): given kinematic human

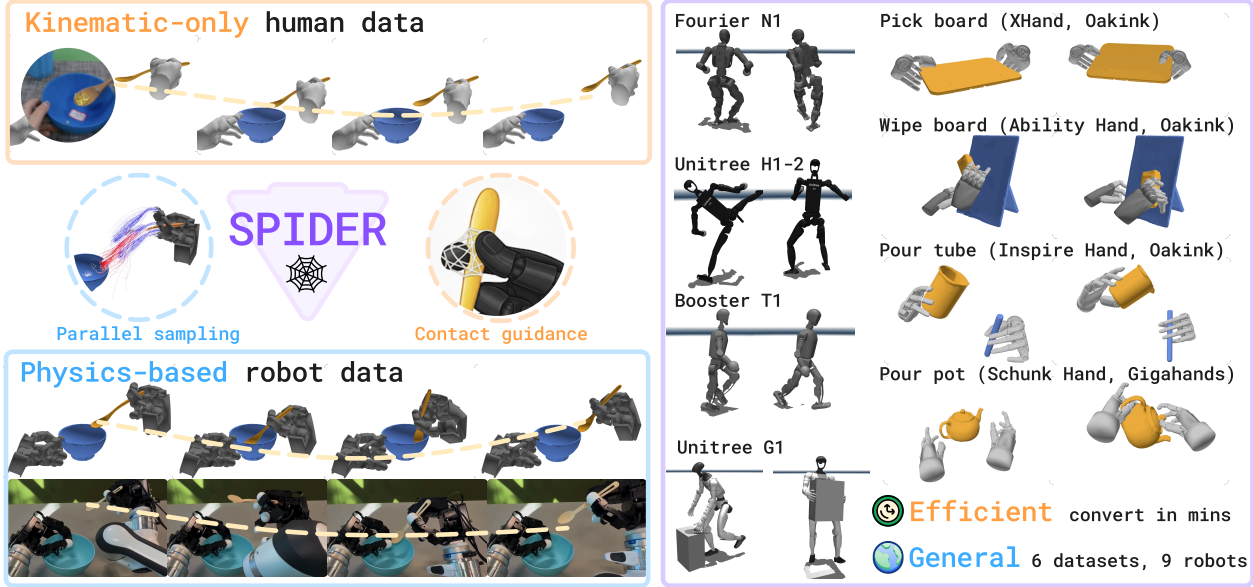


**Figure 1 Overview of SPIDER method.** SPIDER converts human-object interaction trajectories to dynamically feasible robot-object interaction trajectories using sampling with parallel physics simulator. We introduce an additional virtual contact guidance method to minimize the solution ambiguity in contact-rich tasks. With the combination of the two, SPIDER converts human dataset to deployable robot data at scale and supports multiple distinct robot embodiments and task domains.

demonstrations, generate robot motions that (a) align the robot’s poses with human poses, (b) establish consistent contact with the environment, and (c) preserve the task objectives of the demonstrated behavior. The problem presents three key challenges: (a) *Dynamical feasibility*: There is a substantial embodiment gap between humans and robots, and reconstructed demonstrations from mesh estimation and state tracking are often noisy, making direct kinematic transfer infeasible. (b) *Scalability and efficiency*: The abundance of internet-scale human data requires approaches that are both computationally efficient and scalable to large datasets. (c) *Robustness and missing contact information*: Most human datasets lack the force and contact data required to ensure dynamical feasibility and preserve manipulation intent. Existing methods struggle to bridge these gaps: inverse-kinematics (IK) approaches (Qin et al., 2022; Yin et al., 2025a) are efficient but dynamically infeasible; reinforcement learning (RL) approaches (Li et al., 2025c; Lum et al., 2025) are general but requires expensive trajectory-specific training and tedious reward engineering; teleoperation (Yin et al., 2025b) is dynamically feasible but often labor-intensive and embodiment-specific.

To achieve scalable, general, and flexible physics-based cross-embodiment retargeting, we propose Scalable Physics-Informed Dexterous Retargeting (**SPIDER**), a sampling-based approach with contact guidance. Our key insight is that human demonstrations provide high-level guidance in terms of robot motion and task specification, while sampling in simulation grounds trajectories with physics to ensure dynamical feasibility and contact correctness. To reduce contact ambiguity during sampling, we introduce a virtual contact guidance mechanism: a virtual force is added between the robot and the object to “stick” the object to the desired contact point in the initial stage, and is gradually relaxed as the optimization progresses. Importantly, the framework is embodiment-agnostic and task-general: it can be applied to any robot-environment interaction as long as the scene can be simulated.

**Contributions.** Our contributions are summarized as follows:

- We introduce **SPIDER**, a flexible and general physics-informed retargeting framework that scales across six datasets, nine distinct robot morphologies, and two task domains (dexterous hand and humanoid).
- We propose a contact-aware scheme that incorporates object- and environment-centric guidance to preserve manipulation and locomotion intent. It improves the success rate by 18% compared to the baseline and increases retargeting speed by an order of magnitude compared to RL-based methods.

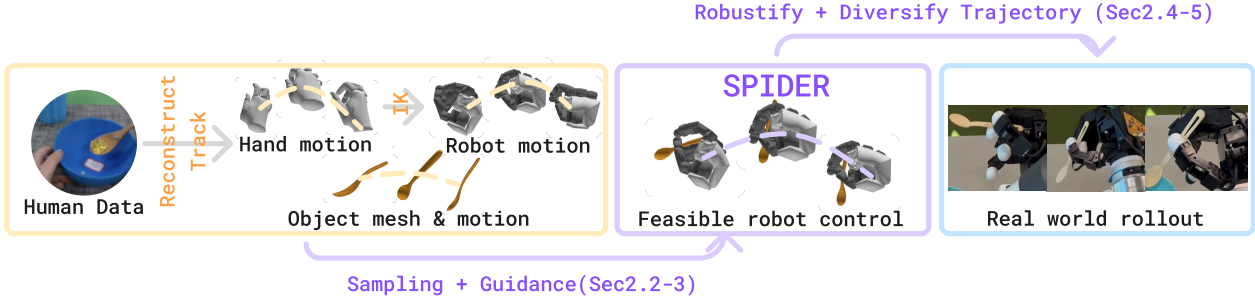


**Figure 2 Overview of the SPIDER pipeline.** The pipeline takes reconstructed object meshes, reference robot motion, and object motion and converts them into a dynamically feasible robot trajectory with corrected contacts. The generated trajectory is further robustified and augmented before deployment or policy learning.

- Our pipeline enables the generation of large-scale, robot-feasible datasets, with 262 episodes, 800 hours of data, and 2.4M frames across five distinct robotic hands and 103 different objects, derived from human data. We release the full data generation pipeline to assist future research.
- **SPIDER** is further extended for downstream applications, such as robustifying trajectories for direct real-robot deployment, augmenting a single demonstration to diverse physical environments/objects, and boosting the learning process of RL policies.

## 2 Physics-based Retargeting with Sampling

This section introduces our pipeline for retargeting human manipulation data to physical robot demonstrations, as illustrated in [figure 2](#). We first formulate the physics-based retargeting problem in [section 2.1](#), followed by its sampling-based solver design in [section 2.2](#). Then, we further improve sampling efficiency and quality with virtual contact guidance in [section 2.3](#). Finally, to handle model mismatch between simulation and reality, we introduce a robustification strategy in [section 2.4](#).

### 2.1 Physics-based Retargeting Problem

We formulate physics-based retargeting as a constrained optimization problem where a robot control sequence  $u_{0:T-1}$  is optimized to minimize the distance to the reference trajectory  $x_{0:T}^{\text{ref}}$  and the control effort. As *input*, a kinematic reference state sequence  $x_t^{\text{ref}}, \forall t \in \{0, \dots, T\}$  is first provided from human demonstrations. The state  $x_t^{\text{ref}} = \{q_t^{\text{ref}}, \dot{q}_t^{\text{ref}}\}$  is composed of reference position  $q_t^{\text{ref}}$  and velocity  $\dot{q}_t^{\text{ref}}$ , where  $q_t^{\text{ref}} = \{q_t^{\text{ref,robot}}, q_t^{\text{ref,object}}\}$ . Specifically, for robots with  $n_u$  joints, its reference position  $q_t^{\text{ref,robot}}$  is composed of robot joint position  $q_t^{\text{ref,joint}} \in \mathbb{R}^{n_u}$  and its base transformation  $T_t^{\text{ref,base}} \in \text{SE}(3)$ . The object reference motion is  $q_t^{\text{ref,object}} \in \text{SE}(3)$ . Physics-based retargeting will *output* a dynamically feasible control sequence of the robot  $u_{0:T-1}$  to minimize the distance to the reference trajectory and the control effort:

$$\min_{u_{0:T-1}} J(u_{0:T-1}) = \min_{u_{0:T-1}} \|x_T - x_T^{\text{ref}}\|_{Q_T}^2 + \sum_{t=0}^{T-1} \left( \|x_{t+1} - x_{t+1}^{\text{ref}}\|_{Q_t}^2 + \|u_t\|_{R_t}^2 \right) \quad (1a)$$

$$\text{s.t. } x_{t+1} = f(x_t, u_t, t) \quad \forall t \in \{0, \dots, T-1\} \quad (1b)$$

$$x_{0:T} \in \mathcal{X}, \quad u_{0:T-1} \in \mathcal{U} \quad (1c)$$

where  $x_{0:T}$  is the optimized feasible state,  $x_{t+1} = f(x_t, u_t, t)$  is the state transition function,  $\mathcal{X}$  is the state space,  $\mathcal{U}$  is the control input space, and  $Q_t$  and  $R_t$  are the state and control input weighting matrices. In practice, we use diagonal weighting matrices for  $Q_t$  and  $R_t$ , where  $Q_t = \text{diag}(\{q_{\text{robot}}, q_{\text{object}}\})$  and  $R_t = \text{diag}(\{r_{\text{robot}}, r_{\text{object}}\})$ .

## 2.2 Sampling for Physics-based Retargeting

Due to the contact-rich nature of physics-based retargeting, the optimization problem in [equation \(1a\)](#) is highly non-convex and often non-continuous. Sampling-based optimization ([Mannor et al., 2003](#)) provides a natural way to handle such landscapes, as it does not rely on smoothness or convexity assumptions. Intuitively, this resembles RL in that both rely on sampled trajectories from parallelized simulation to guide decision-making, but instead of updating a policy network, we directly use the samples to optimize the control sequence  $U = u_{0:T-1}$ . To this end, we adopt a sampling-based optimizer with an annealed sampling kernel ([Xue et al., 2025; Pan et al., 2024](#)):

$$U^{i+1} = U^i + \frac{\sum_{j=1}^{N_W} \exp\left(-\frac{J(U^i + [W]_j)}{\lambda}\right) [W]_j}{\sum_{j=1}^{N_W} \exp\left(-\frac{J(U^i + [W]_j)}{\lambda}\right)}, \quad (2)$$

$$\Sigma_h^i = \exp\left(-\frac{N-i}{\beta_1 N} - \frac{H-h}{\beta_2 H}\right) I, \quad (3)$$

where  $U^i$  is the solution at iteration  $i$ ,  $i = 1, \dots, N$  is the iteration index with  $N$  being the total number of iterations,  $[W]_j \sim \mathcal{N}(0, \Sigma_{0:H-1})$ ,  $j = 1, \dots, N_W$  is sampled  $N_W$  Gaussian noise with scheduled covariance  $\Sigma_h$ ,  $h \in \{0, \dots, H-1\}$ ,  $\beta_1, \beta_2 \in (0, 1)$  are annealing parameters controlling sampling covariance in line 6 of [algorithm 1](#).

---

### Algorithm 1 Sampling for Physics-based Retargeting

---

```

1: Input:  $x_{0:T}^{\text{ref}}$ ,  $U^0$ ,  $H$ ,  $N_W$ ,  $\lambda$ ,  $\beta_1, \beta_2$ ,  $N$ ,  $\epsilon_{\text{tol}}$ 
2:  $J_{\text{best}} \leftarrow \infty$ ,  $i \leftarrow 0$ 
3: while  $i < N$  and not converged do
4:    $i \leftarrow i + 1$ ; Update  $\Sigma_h^i$  using equation \(3\) ▷ Annealing schedule for sampling covariance
5:   for  $j \in \{1, \dots, N_W\}$  do
6:     Sample  $[W]_j \sim \mathcal{N}(0, \Sigma_{0:H-1})$ ;  $[U^i]_j \leftarrow U^i + [W]_j$ 
7:     Compute  $J([U^i]_j)$  by simulation rollout (equation \(1a\))
8:   end for
9:   Update  $U^{i+1}$  using weighted average from equation \(2\)
10:  if  $|J_{\text{best}} - \min_j J(U_j)| < \epsilon_{\text{tol}}$  then
11:    break ▷ Early stop if improvement is small
12:  end if
13:   $J_{\text{best}} \leftarrow \min_j J(U_j)$ 
14: end while
15: Return  $U^*$ 

```

---

In contact-rich dexterous manipulation, the *feasible solution set is typically narrow*, so effective optimization requires a combination of *coarse search* to discover feasible contact modes and *fine refinement* to achieve stable contact. The annealed sampling covariance in [equation \(2\)](#) implements this exploration-exploitation trade-off:  $\beta_1$  controls the rate across outer iterations (global-to-local search over optimization updates), and  $\beta_2$  controls the rate along the prediction horizon (allocating more or less perturbation across timesteps). As the schedule progresses, the effective sampling radius transitions from broad exploration to targeted exploitation around promising trajectories. [Figure 3](#) illustrates this effect: unlike standard sampling (e.g. MPPI) using a fixed search radius, annealed sampling shrinks the radius in later iterations, effectively reducing the variance of the sampled trajectories. To further improve speed, we adopt an early stopping strategy ([Kamat et al., 2022](#)), where optimization halts when improvements from further sampling become small. [Algorithm 1](#) presents a base sampling framework for physics-based retargeting.

## 2.3 Virtual Contact Guidance

**Solutions Ambiguity.** For a retargeting method to be valid, it is also important to preserve the human-preferred contact in the demonstration. Take the stir stick manipulation in [figure 3](#) as an example, the robot can hold

the stick either between the thumb and index finger or between the index and middle finger; both achieve the task, but the former is more natural and aligns with the human demonstration. However, due to the non-convex cost landscape of [equation \(1a\)](#) there may be multiple solutions that achieve similar object motion with different contact behaviors. As a result, a sampling-based optimizer may converge to alternative contact modes, leading to implausible contact trajectories in a demonstration even when the object trajectory is reproduced.

**Virtual Contact Guidance.** To guide sampling towards the desired contact mode, we introduce *virtual*

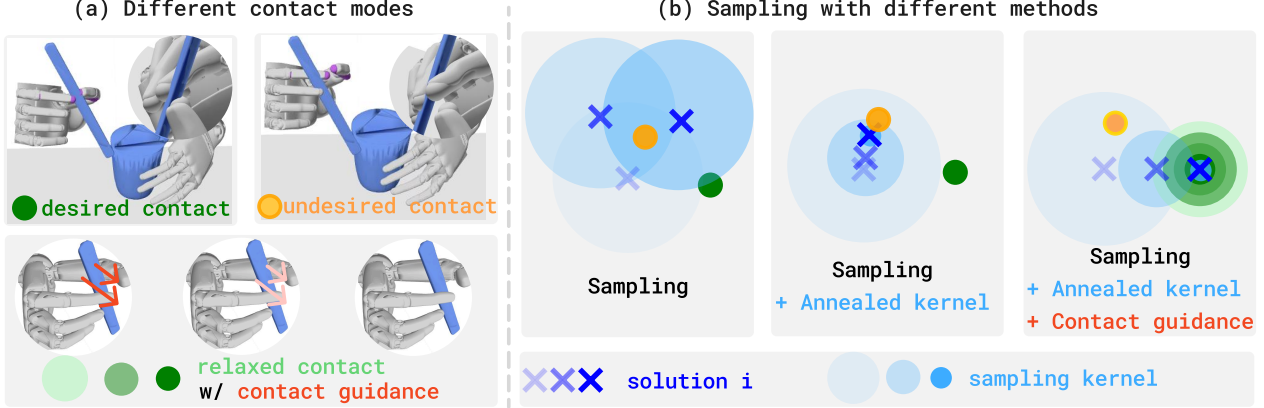


**Figure 3 Contact mode mismatch in sampling and virtual guidance method to correct it.** (a) Given the same task, the robot can hold the object in different contact modes while still finishing the task. However, the contact mode from human is preferred. (b) Given different sampling methods when seeking a feasible motion with correct contact: *Standard sampling* (left): uses a fixed search radius, leading to high variance. The resulting solution fails to converge well. *Annealed sampling* (middle): gradually shrinks the search radius, starting coarse and narrowing down to a finer solution, but may drift toward a feasible solution with wrong contact. *Annealed sampling with virtual contact guidance* (right): expands the feasible region by adding virtual guidance near target contacts. This enlarges the feasible region to a relaxed feasible set, steering sampling away from undesired feasible solutions and towards the intended contact sequence.

*contact guidance.* This guidance factor expands the feasible solution set and biases the optimization process towards the target configuration. Unlike a soft contact reward or cost - which may still fail when the desired mode is harder to sample - virtual contact guidance explicitly *enlarges* the basin of attraction to make it easier to sample from, as illustrated in [figure 3](#). Our method applies a virtual constraint between intended contact points on the object and robot fingers, “sticking” the object to the target configuration in early stages and gradually relaxing this constraint in a curriculum-like fashion. Concretely, we impose a virtual constraint that maintains the relative position between contact pairs. For the  $k$ -th object-hand contact pair (e.g., handle-thumb), we define the current relative position as  ${}^{\text{robot}}p_{k,t}^{\text{object}} = p_{k,t}^{\text{robot}} - p_{k,t}^{\text{object}}$  and the desired reference position as  ${}^{\text{robot}}p_{k,t}^{\text{object,ref}} = p_{k,t}^{\text{robot,ref}} - p_{k,t}^{\text{object,ref}}$ . The constraint is activated when the contact indicator  $c_{k,t} = 1$ , which occurs when the reference relative position is within the contact threshold:  $c_{k,t} = \mathbf{1}(\|{}^{\text{robot}}p_{k,t}^{\text{object,ref}}\|_2 \leq \epsilon_{\text{contact}})$ . The constraint strength is controlled by a penalty parameter  $\eta_i \rightarrow \infty$  when  $i \rightarrow N$ :

$$c_{k,t} \|{}^{\text{robot}}p_{k,t}^{\text{object}} - {}^{\text{robot}}p_{k,t}^{\text{object,ref}}\|_2^2 \leq \eta_i \quad (4)$$

This strategy connects to prior ideas: virtual object constraint ([Mandi et al., 2025](#))  $\|p_{k,t}^{\text{object}} - p_{k,t}^{\text{object,ref}}\|_2^2 \leq \eta$ , which expands feasibility around absolute object states in RL, and contact cost ([Lakshminipathy et al., 2025](#)), biasing optimization towards desired hand-object *relative* states. Our formulation reduces sampling complexity while preserving the intended contact sequence by maintaining *relative* hand-object relationships.

**Robustness against imperfect reference contact.** It is important to note that, in order to maintain robustness against imperfect demonstrations with noisy or unstable contact, virtual constraints should be selectively relaxed rather than enforced indiscriminately. To achieve this, we apply a contact filter that detects unstable interactions: if a contact duration is shorter than  $t_{c,\min}$  or if the contact point drifts more than  $d_{c,\max}$  during that period, the contact is classified as unstable and the corresponding virtual constraint is disabled.

This implementation ensures that only reliable contacts contribute to guidance, thereby preventing noisy demonstrations from biasing the optimization process.

## 2.4 Trajectory Robustification

**Handling imperfection in reference motion.** To bridge the gap from reconstructed demonstrations to real hardware, we robustify trajectories against unknown or misspecified dynamics (e.g., friction, contact compliance) and reconstruction noise (e.g., object mesh estimation error, pose estimation error) that could otherwise make a nominal plan infeasible. Our approach optimizes a control sequence with a pessimistic (min–max) objective over a bounded parameter set  $\mathcal{D}$ , similar to domain randomization (DR) method (Tobin et al., 2017) but replacing expectation with worst-case cost to ensure universal feasibility:

$$J_{\text{rob}}(U) = \max_{d \in \mathcal{D}} J(U, d), \quad (5)$$

where  $J(U, d)$  is the cost in equation (1a) under dynamics parameter  $d$ . In practice,  $\mathcal{D}$  spans variations such as contact margin size, friction coefficients, and object mass. During optimization, each candidate sequence  $U_j$  is rolled out over a mini-batch  $d_{1:K} \sim \mathcal{D}$  and evaluated by  $\max_{k \leq K} J(U_j, d_k)$ , following robust sampling-based control (Williams et al., 2018). This formulation integrates seamlessly with the update rule in equation (2), leverages GPU parallelization through batched rollouts, and has minimum computational overhead.

## 2.5 Physics-based Data Augmentation

Apart from generating feasible robot actions, another advantage of physics-based retargeting is the ability to systematically augment the retargeted data with diverse *physics-aware* behaviors. Starting from a single human demonstration, **SPIDER** is capable of diversifying a single behavior into a diverse set of physically feasible actions which could be used for downstream training (Mandlekar et al., 2023; Jiang et al., 2025; Yin et al., 2025b).

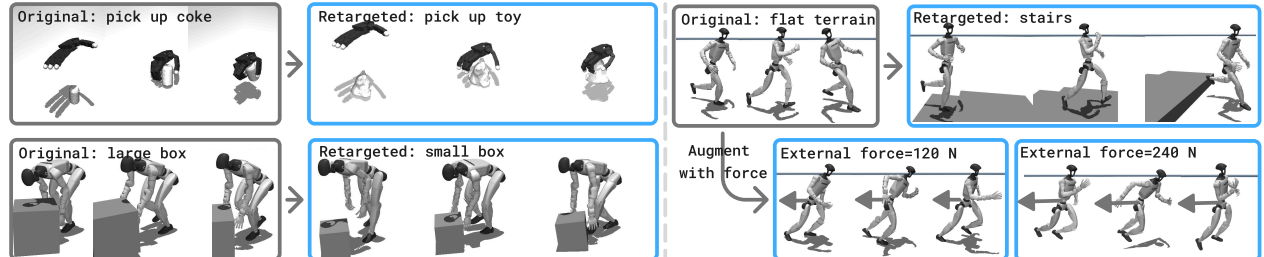


**Figure 4 Physics-based data augmentation.** We augment the retargeted data from a single demonstration into a diverse set of physically feasible actions. Here we demonstrate (a) generating motion with new object mesh for dexterous manipulation, (b) moving a lighter and smaller object for humanoid robot tasks, (c) adding stairs to the scene for humanoid running motion. (d) applying external forces to the robot when it is pulling a heavy object.

**Geometric Variations.** **SPIDER** supports generating diverse geometric variations of the objects while still grounding it with physics. For dexterous manipulation tasks, we perturb the initial object pose and scale to generate diverse interaction behaviors while the reference motion is kept the same. We can even directly replace the object mesh with a different one to generate new interaction behaviors. For instance, in figure 4, we augment the grasping motion of a coke to a cat toy simply by replacing the object mesh. Similarly, the same idea can be applied to human-object interaction for humanoid robot tasks. By modifying the object geometry to make it smaller and lighter, the robot can automatically adapt to the new object by lowering the body down and switching to single-hand pushing motion with smaller force. One can also change the terrain to stairs to transform a running in flat ground motion into a running on stairs motion, which is challenging for kinematic-only retargeting due to climbing stairs requires new contact patterns.

**Physics Variations.** The distinct advantage of **SPIDER** as a physics-based approach is to be force-aware. We demonstrate the ability of **SPIDER** to generating new behaviors by applying external forces to the robot when it is pulling a heavy object. A large force (120N and 240N respectively, where the gravity is 320N) is applied

to pull the robot back. With physics-based retargeting, the generated trajectory is able to resist the force by leaning forward and moving slower, as demonstrated in [figure 4](#).

### 3 Performance Evaluation

This section numerically evaluates the proposed method with settings detailed in [section 3.1](#). First, in [section 3.2](#), we ablate the effect of the annealed kernel and virtual contact guidance in sampling and compare them with the kinematic-retargeting baseline. Then, to provide a quantitative assessment of generated motion quality, we compare **SPIDER** with state-of-the-art retargeting baselines on dexterous manipulation [section 3.3](#) and humanoid whole-body control [section 3.4](#).

#### 3.1 Experimental Setup

**Dataset Selection.** For dexterous manipulation tasks, we evaluate on 3 bimanual manipulation datasets: **GigaHands** ([Fu et al., 2025](#)), **Oakink** ([Zhan et al., 2024](#)) and **ARCTIC** ([Li et al., 2023](#)), comprising in total 1262 episodes and 2.4M frames across five distinct robotic hands and 103 different objects. For humanoid tasks, we choose commonly used **LAFAN1** ([Harvey et al., 2020](#)), **AMASS** ([Mahmood et al., 2019](#)) for locomotion and **OMOMO** ([Li et al., 2023](#)) dataset for human-robot interaction. To the best of our knowledge, **SPIDER is the first universal retargeting method that can handle both dexterous manipulation and humanoid whole-body control tasks at this scale.**

**Robot Embodiments.** For dexterous manipulation, we evaluate across 5 different robotic hands to demonstrate the generalizability of our method: **Allegro**, **XHand**, **Inspire**, **Ability**, and **Schunk**. On humanoid whole-body control tasks, we use **Unitree G1**, **Unitree H1-2**, **Fourier N1** and **Booster T1** as the target embodiment. These platforms exhibit significant variations in degrees of freedom, dimensions, and finger configurations (see [figure 5](#)), showcasing our method’s cross-embodiment capabilities.

Robot	(a) Dexterous hand					(b) Humanoid			
	Allegro	Schunk	Xhand	Inspire	Ability	Unitree	Unitree	N1	T1
Length	26.0cm	24.2cm	19.5cm	15.6cm	14.6cm	Unitree	Unitree	N1	T1
Dof	16	20	12	12	12	26	29	23	23

**Figure 5 Specifications of robots used in evaluation.** **SPIDER** supports both dexterous hand and humanoid robot. The significant variations in DoF, dimensions, and finger count demonstrate the cross-embodiment generalizability of our approach. We employ a simulated 12-DoF configuration ([Li et al., 2025c](#)) of the **Inspire** and **Ability** hands, removing the joint constraints compared to their real-world versions.

**Evaluation Metrics.** For dexterous manipulation and humanoid-object interaction tasks, we evaluate tracking performance on the object motion, since the goal is to move the object rather than to precisely track the robot hand. For object tracking error, we compute per-step averaged rotation error  $E_{\text{rot}} = \frac{1}{T} \sum_{t=1}^T \arccos(2\langle q_{\text{obj},t}, q_{\text{obj},t}^{\text{ref}} \rangle^2 - 1)$  and position error  $E_{\text{pos}} = \frac{1}{T} \sum_{t=1}^T \|p_{\text{obj},t} - p_{\text{obj},t}^{\text{ref}}\|_2$ , where  $T$  is the number of timesteps,  $q_{\text{obj},t}$  and  $p_{\text{obj},t}$  are the object quaternion and position at timestep  $t$ , respectively. We follow the same evaluation setting as **ManipTrans** ([Li et al., 2025c](#)) and **DexMachina** ([Mandi et al., 2025](#)), where we report task success only concerning object motion. Task success is defined using: (1) the rotation error  $E_{\text{rot}} < 0.5$  rad, and (2) the average per-step translation error  $E_{\text{pos}} < 0.1$  m. For humanoid locomotion, the joint tracking error, pelvis position error and pelvis orientation error are computed.

### 3.2 Ablation Study

To ensure representative evaluation while maintaining computational feasibility, we conduct our ablation study on a collection of challenging manipulation tasks from established datasets: (1) for **Oakink** (Zhan et al., 2024), we evaluate on 7 distinct bimanual two-object manipulation tasks that were previously benchmarked in **ManipTrans** (Li et al., 2025c); and (2) for **GigaHands** (Fu et al., 2025), we utilize their released example dataset comprising 3 manipulation trajectories.

**Baseline Selection.** We compare four approaches: (1) **Kinematic** retargeting: fingertip inverse kinematics as an initial-guess quality baseline; (2) vanilla **Sampling** (based on **MPPI** (Howell et al., 2022)): standard sampling-based control; (3) **Sampling** with an annealed kernel (similar to **DIAL-MPC** (Xue et al., 2025)): differs from our method only in the absence of virtual guidance; and (4) **Sampling** with an annealed kernel and virtual contact guidance (our full method). We exclude RL-based comparisons here since they produce policies rather than direct control sequences, making direct comparison inappropriate. RL methods are evaluated separately in [section 3.3](#) for motion quality assessment.

Dataset	Robot	Kinematic	Sampling	Sampling +annealing	Sampling +annealing +contact
Oakink (Zhan et al., 2024)	Ability	0.13	0.30	0.43	<b>0.54</b>
	Allegro	0.13	0.40	0.69	<b>0.85</b>
	Inspire	0.10	0.23	<b>0.45</b>	<b>0.45</b>
	Schunk	0.0	0.28	<b>0.54</b>	0.53
	XHand	0.10	0.35	0.71	<b>0.77</b>
GigaHands (Fu et al., 2025)	Ability	0.0	0.32	0.73	<b>0.80</b>
	Allegro	0.0	0.40	<b>1.00</b>	<b>1.00</b>
	Inspire	0.0	0.36	0.67	<b>0.93</b>
	Schunk	0.0	0.64	0.93	<b>1.00</b>
	XHand	0.0	0.40	<b>1.00</b>	<b>1.00</b>

**Table 1 Ablation study success rates across different datasets and robot hands.** Results evaluated on eight example trajectories of **Oakink** from **ManipTrans** and five example trajectories of **GigaHands** over five seeds. Sampling with both annealing and contact guidance consistently achieves the highest success rates across all robot-dataset combinations.

**Key Findings.** Key results are presented in [table 1](#), where sampling equipped with an annealed kernel and virtual contact guidance consistently achieves the highest success rates across all robot-dataset combinations, outperforming the annealed-kernel-only version by  $\sim 18\%$ . The annealed-kernel-only version is faster, achieving 3.0 Hz compared to 2.5 Hz for the full version.

### 3.3 Dexterous Manipulation Retargeting Results

**Retargeted Dataset Quality.** To validate the quality of the generated data on large scale dataset, we first report the success rates on full dataset used the same metrics as in [section 3.2](#). Full results are shown in [table 2](#), where we demonstrate the first large-scale retargeting evaluation across such diverse embodiments and datasets. Across datasets, **GigaHand** demonstrates higher success rates due to its focus on pick-and-place motions, which are inherently more amenable to retargeting. In contrast, **Oakink** presents greater challenges as objects are often pre-grasped, making success heavily dependent on achieving precise initial contact configurations. Across robot embodiments, hands with higher degrees of freedom (e.g., **Inspire**, **Allegro**) are generally easier to retarget as the additional actuators provide greater flexibility. [Figure 6](#) shows some example trajectories generated by **SPIDER** on different hands.

**Baselines and Reference Methods.** We compare against state-of-the-art policy-learning systems where available: **ManipTrans** (Li et al., 2025c) on **Oakink** and **DexMachina** (Mandi et al., 2025) on **ARCTIC**. Unlike these methods, which train policies, our approach directly optimizes control, so the comparison serves only as a performance reference. Generation efficiency is measured by Frames Per Second (FPS), defined as the number of frames in a trajectory divided by computation time. Matching FPS to the reference trajectory

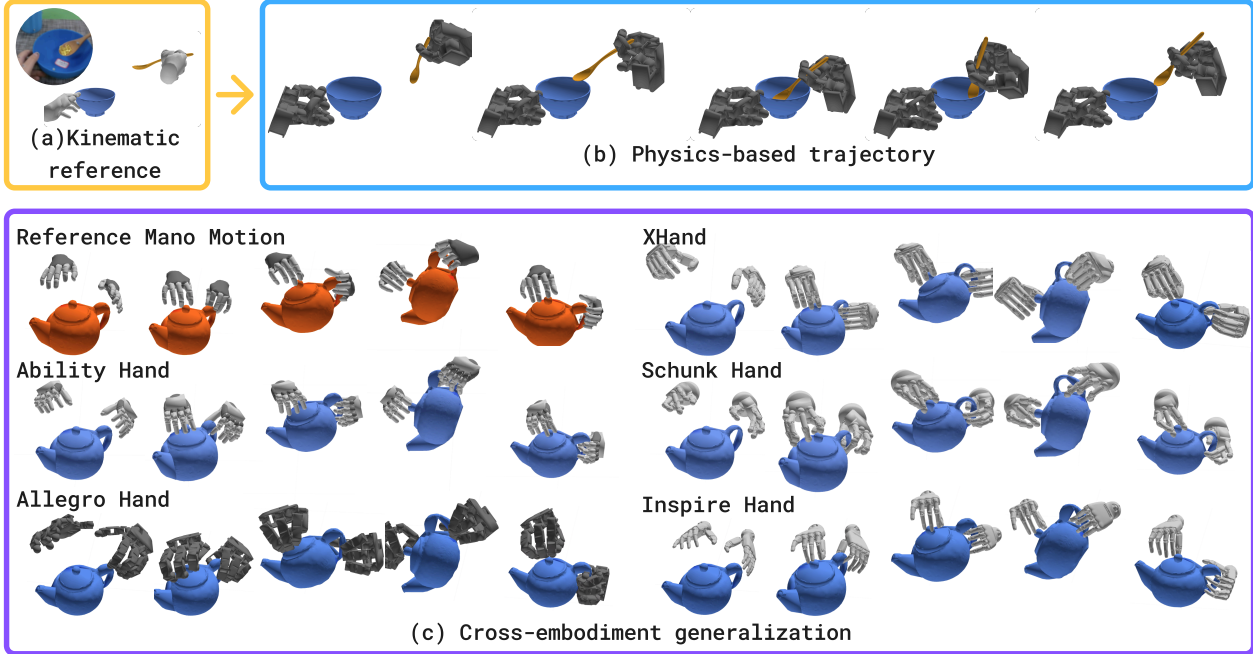


**Figure 6 Retargeted dexterous manipulation trajectories on different hands.** Starting with an infeasible motion with penetration and infeasible contact, **SPIDER** grounds it with physics. Different hands adapt different behaviors with the same sampling parameters.

Dataset	# Traj.	Ability	Allegro	Inspire	Schunk	XHand
Oakink (Zhan et al., 2024)	1022	0.413	0.459	<b>0.479</b>	0.431	0.422
GigaHands (Fu et al., 2025)	756	0.741	0.810	<b>0.879</b>	0.706	0.812

**Table 2 Success rates of SPIDER across different datasets and robot hands on the *full* dataset.** Different hands have various success rates due to their size and dof differences. Both **Inspire** and **Ability** hands use 12-DoF simulation model instead of the original one.

frequency indicates real-time generation; lower values indicate slower speeds. **Table 3** show that **SPIDER** achieves competitive success rates on simpler **Oakink** tasks but lags on more complex **ARCTIC** manipulations. Its main advantage is speed: trajectory generation is an order of magnitude faster, enabling large-scale dataset retargeting and potential online applications.

**Deployment Results.** To demonstrate the dynamical feasibility of our retargeted trajectories, we deploy **SPIDER** on a physical system consisting of a 7-DoF **Franka Emika Panda** with an **Allegro** hand, requiring no additional adaptation beyond the robustification strategies in [section 2.4](#). The arm is controlled using operational space control (OSC), while the hand directly executes the optimized joint actions from our method. We evaluate performance on four dexterous manipulation tasks—rotating a light bulb, manipulating a small spoon, playing a guitar, and unplugging a charger—each demanding precise finger coordination and showcasing the practical applicability of our retargeting approach. Representative execution sequences are shown in [figure 7](#). The successful execution of these tasks validates that trajectories optimized in simulation with virtual constraints can be transferred directly to real hardware while preserving the precision required for delicate manipulation.

### 3.4 Humanoid Whole-Body Control Retargeting Results

As a universal physics-based retargeting method, **SPIDER** is versatile and can be applied to various robot embodiments, including humanoid robots. To adapt **SPIDER** for humanoid robots, virtual contact guidance is implemented between the robot’s feet and the floor. In [figure 8](#), we showcase the application of **SPIDER**

Method	Dataset	# Traj.	Success ↑	FPS ↑
SPIDER	Oakink	1022	<b>47.9%</b>	<b>2.5</b>
ManipTrans	Oakink	80*	39.5%	0.1
SPIDER	ARCTIC	7	42.0%	<b>1.5</b>
DexMachina	ARCTIC	7	<b>67.1%</b>	0.05

**Table 3 Retargeted Data Quality Comparison.** Comparison of generated trajectory quality between our sampling-based method and RL-based baselines on the *Inspire* hand since this is the one used by **ManipTrans**. To unify the comparison, we only compare the generated trajectories, not the policies themselves. **SPIDER** achieves competitive task success rates while maintaining one order of magnitude faster generation speed. \***ManipTrans** results are from their released dataset as they did not report which specific trajectories were used for retargeting.

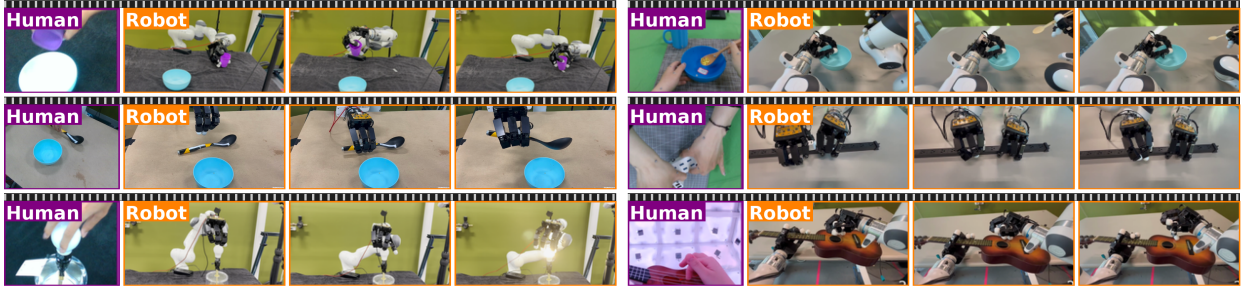


**Figure 7 Open-loop rollout with robustification.** Left: showing single-arm tasks including pouring a cup, pick a spoon and rotating a light bulb. Right: showing dual-arm tasks including scooping a bowl, unplug a charger and playing a guitar. The retargeted trajectories are executed directly on the physical robot.

on the humanoid **AMASS** (Mahmood et al., 2019) and **LAFAN1** (Harvey et al., 2020) datasets. The retargeting process corrects artifacts such as foot penetration and slipping, enabling the robot to execute highly dynamic motions, as illustrated in figure 8, which shows an *open-loop rollout* of the retargeted control and highlights the dynamical feasibility of the retargeted motion. We compare **SPIDER** with popular kinematics-based retargeting method, named general motion retargeting (**GMR**) (Araujo et al., 2025).

Dataset	Method	Joint Err. ↓	Pos. Err. ↓	Ori. Err. ↓	Obj. Pos. Err. ↓	Obj. Ori. Err. ↓	FPS ↑
LAFAN1	GMR	1.08	2.01	2.40	N/A	N/A	<b>35.2</b>
	SPIDER	<b>0.58</b>	<b>0.11</b>	<b>0.07</b>	N/A	N/A	23.1
AMASS	GMR	6.2	4.1	18.7	N/A	N/A	<b>37.2</b>
	SPIDER	<b>0.75</b>	<b>0.23</b>	<b>0.08</b>	N/A	N/A	22.0
OMOMO	GMR	0.57	1.43	2.28	1.18	1.68	<b>28.0</b>
	SPIDER	<b>0.83</b>	<b>0.20</b>	<b>0.17</b>	<b>0.18</b>	<b>0.06</b>	19.6

**Table 4 Tracking Error and FPS Comparison on Humanoid Datasets.** Joint Err.: mean joint angle difference (degrees). Pos. Err.: mean end-effector position error (cm). Ori. Err.: mean end-effector orientation error (degrees). Obj. Err.: mean object pose error (cm or degrees). FPS: trajectory generation speed. Our method achieves the lowest tracking errors and highest FPS compared to **GMR** across all datasets.

## 4 Applications

As a universal physics-based retargeting method, **SPIDER** is compatible with diverse quality data and can be applied to various downstream tasks to get a closed-loop policy. To demonstrate the robustness of **SPIDER** to upstream data quality, **SPIDER** is applied to convert data from single RGB camera video into executable robot trajectories (section 4.1). To showcase the feasibility of **SPIDER** to assist downstream learning tasks, data generated from **SPIDER** is used to train a RL policy for humanoid robots (section 4.2).

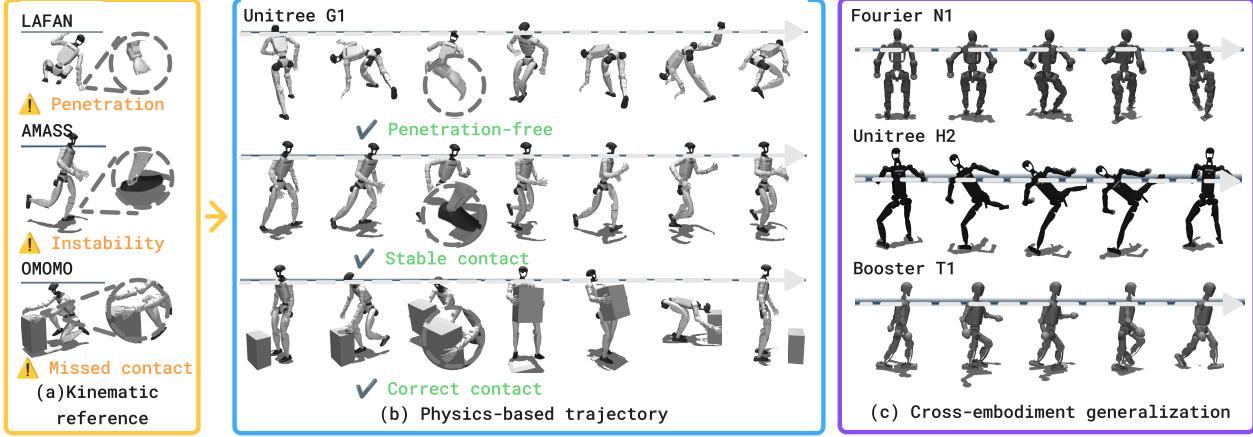


**Figure 8 Open-loop rollout of the retargeted control on diverse humanoid robots with different datasets.** We demonstrate **SPIDER** on the LAFAN1, AMASS and OMOMO datasets. **SPIDER** remove all artifacts from the kinematic trajectory by grounding them with physics and can be applied to various humanoid robots without additional adaptation.

#### 4.1 Retargeting from Single RGB Camera

To demonstrate the flexibility of **SPIDER** for up-streaming data, we evaluate it on converting single RGB camera video into executable robot trajectories. The pipeline consists of: (1) 3D mesh reconstruction with Trellis (Xiang et al., 2025), (2) hand pose estimation with HAMER (Pavlakos et al., 2024) to obtain MANO parameters, and (3) object pose tracking with FoundationPose (Wen et al., 2024) for 6D trajectories. Due to the occlusion and limited resolution, the human and object motion are more noisy than the dataset, which requires more robust physics grounding. As shown in figure 9, we validate on single-hand manipulation tasks like pouring with a cup and installing a bolt. Real-world noise, artifacts, and penetrations are corrected through physics grounding in **SPIDER**, and the retargeted trajectories are directly executable on physical robots.

#### 4.2 Retargeting for RL Policy Training

**RL Policy Training.** For unstable systems like humanoid robots, the generated trajectory is not directly executable on the real robot due to the lack of feedback. One common solution is to train a RL policy to track the generated trajectory (He et al., 2024; Yang et al., 2025a; Liao et al., 2025). However, starting from infeasible human motion, general tracking policy training relies on heavy regularization (Ze et al., 2025; He et al., 2025) and complex curriculum design (He et al., 2024; Li et al., 2025c) to handle the noisy and infeasible reference motion. On the other hand, Liao et al. (2025); Yang et al. (2025a,b) shows with careful retargeting, the policy learning can be easier with less artificial designs. With trajectory retargeted by **SPIDER**, which already comes with a feedforward nominal control and a feasible trajectory, the RL policy only needs to learn a residual feedback term to correct the deviation from the nominal control:

$$u_t = u_t^{\text{SPIDER}} + \pi_\theta(o_t) \quad (6)$$

where  $u_t^{\text{SPIDER}}$  is the nominal control from **SPIDER** and  $\pi_\theta(o_t)$  is the RL policy output at time  $t$ . In practice, we found only joint position tracking reward with object/pelvis pose tracking is sufficient to get a stable motion.

**Training Results on Humanoid Robots.** We evaluate the policy training with the adopted framework from Weng et al. (2025). We take standard practice of training PPO but removing the auxiliary contact reward for simplicity. Figure 10 shows training progress on the OMOMO dataset along side with generated motion. The original human motion is offset from the object position, thus missing the contact. When training with the original human motion, the robot fails to grasp the object and only achieves body tracking goal. On the other hand, the policy trained with **SPIDER** is not only converged faster, but also achieves better object tracking performance. This again highlights the importance of physics grounding for reference motion.

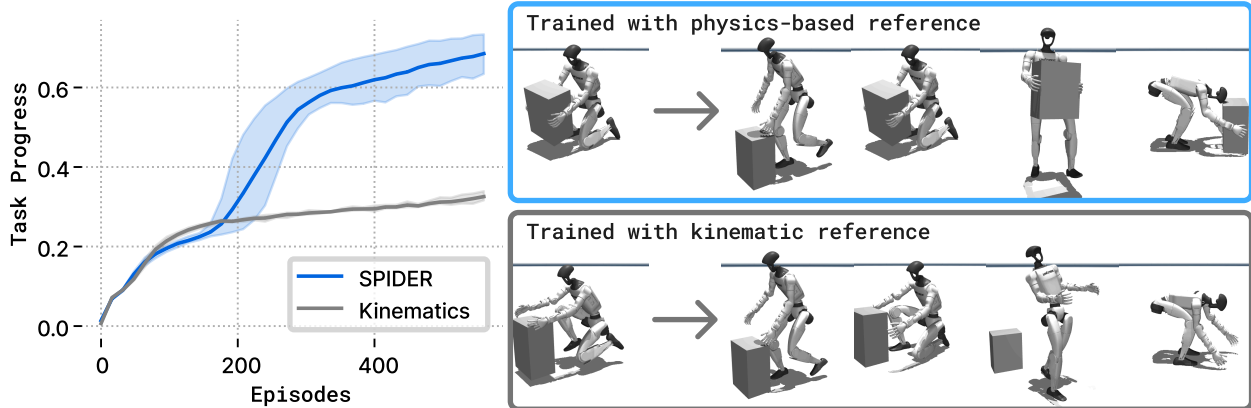


**Figure 10 RL Policy Training on Humanoid Robots.** In reference motion, the robot will first pick up the box and then place it on the floor. Due to the motion capture error, the original reference motion missed the contact with the object. After retargeting with **SPIDER**, the contact is corrected and a feasible feedforward control is provided to assist the policy learning. Left: task progress of the original human motion, demonstrating how many percentage of the target motion is achieved. Right: resulted policy after training.

## 5 Related Work

### 5.1 Learning Manipulation from Human Data

Recent work explores learning robot skills from large-scale human videos by first detecting actions and transferring them to robots. One common strategy is kinematic retargeting, where human poses or keypoints are mapped to robot motions, as in DemoDiffusion (Park et al., 2025), OKAMI (Li et al., 2024), R+X (Papagiannis et al., 2025), and EgoZero (Liu et al., 2025). Another strategy is to train a human-centric policy and then adapt it to robots through fine-tuning with in-domain data, as in MimicPlay (Wang et al., 2023), Track2Act (Bharadhwaj et al., 2024), and VideoDex (Shaw et al., 2022). Our approach is complementary to these pipelines. Specifically, **SPIDER** can serve as a drop-in replacement for the human-to-robot action transfer components, providing more accurate and contact-aware mappings for dexterous and whole-body control.

### 5.2 Retargeting from Human Data

Motion retargeting seeks to convert human data into robot trajectories that are physically consistent and executable.

**Kinematic Retargeting.** These methods map human motion to robot configurations (Qin et al., 2022). While efficient and easy to compute, they often rely on specialized hardware (Xu et al., 2025), handcrafted motion primitives (Wu et al., 2024), and struggle with realism in contact-rich tasks (Qin et al., 2023). Being kinematic only, the generated motions are not compliant with physics constraints.

**Learning-Based Retargeting Networks.** Neural mapping approaches train networks to convert human motions into robot motions (Park et al., 2025; Yin et al., 2025b). Such models can outperform direct kinematic mappings and retain fast inference, but they require extensive pretraining and may fail when facing out-of-distribution motions or novel embodiments.

**Optimization-Based Retargeting.** Optimization-based approaches explicitly incorporate physics and contact constraints to ensure dynamical feasibility (Reda et al., 2023). They can generate high-quality, physically plausible motions, but often depend on detailed contact data (Lakshmpathy et al., 2025), specific data pipelines (Yang et al., 2025b), and strong priors (Nakaoka et al., 2005). Due to the non-convex nature of the problem, sampling-based approaches (Yang et al., 2025b; Si et al., 2025) have emerged as a promising solution.

**RL-Based Retargeting.** RL has been used to retarget human demonstrations across embodiments (Lum et al., 2025; Li et al., 2025c). When combined with curriculum learning (Mandi et al., 2025; Liu et al., 2024), RL can produce dexterous, physically feasible robot motions. However, it typically requires training on each trajectory and significant computation, which limits scalability to internet-scale data and real-time deployment.

Existing methods trade off between efficiency (kinematics, neural networks) and physical fidelity (optimization, RL). **SPIDER** combines the generality of RL with the efficiency of optimization-based pipelines, making it a scalable and practical drop-in replacement for human-to-robot transfer.

### 5.3 Sampling-based Optimization for Robot Control

Sampling-based optimization methods such as the cross-entropy method (De Boer et al., 2005), evolutionary algorithms (Salimans et al., 2017), and Bayesian optimization (Frazier, 2018) are powerful tools for solving non-convex and non-smooth problems. Due to their parallelizability and flexibility, these methods have been applied to navigation (Williams et al., 2016), legged locomotion (Xue et al., 2025), and dexterous manipulation (Howell et al., 2022; Li et al., 2025a). Despite their success in contact-rich control, they can suffer from instability and solution ambiguity in trajectory sampling (Kim et al., 2022). **SPIDER** addresses these challenges by guiding sampling with contact information, which helps preserve the intended contact sequence.

## 6 Conclusion and Future Work

This paper introduces **SPIDER**, a flexible and efficient physics-based retargeting framework that enables large-scale robot demonstration generation from human data. **SPIDER** achieves competitive performance compared to state-of-the-art methods while being an order of magnitude faster. Despite its generality, **SPIDER**’s performance depends on the quality of reconstructed 3D human-object interaction data; noisy meshes and motion can yield degraded trajectories. As one promising application, **SPIDER** can be applied to behavior cloning pipeline to unlock generalizable dexterous manipulation policies.

## Acknowledgements

Chaoyi Pan thanks Mandi Zhao for her help in integrating **DexMachina** into the framework, and thanks Haoyang Weng for the support for the humanoid-object interaction integration from **HDMI**. Guanya Shi holds concurrent appointments as an Assistant Professor at Carnegie Mellon University and as an Amazon Scholar. This paper describes work performed at Carnegie Mellon University and is not associated with Amazon.

## References

Joao Pedro Araujo, Yanjie Ze, Pei Xu, Jiajun Wu, and C. Karen Liu. Retargeting matters: General motion retargeting for humanoid motion tracking. *arXiv:2510.02252*, 2025.

Homanga Bharadhwaj, Roozbeh Mottaghi, Abhinav Gupta, and Shubham Tulsiani. Track2act: Predicting point tracks from internet videos enables generalizable robot manipulation. In *ECCV*, 2024.

Anthony Brohan, Noah Brown, Justice Carbajal, Yevgen Chebotar, Xi Chen, Krzysztof Choromanski, Tianli Ding, Danny Driess, Avinava Dubey, Chelsea Finn, Pete Florence, Chuyuan Fu, Montse Gonzalez Arenas, Keerthana Gopalakrishnan, Kehang Han, Karol Hausman, Alexander Herzog, Jasmine Hsu, Brian Ichter, Alex Irpan, Nikhil Joshi, Ryan Julian, Dmitry Kalashnikov, Yuheng Kuang, Isabel Leal, Lisa Lee, Tsang-Wei Edward Lee, Sergey Levine, Yao Lu, Henryk Michalewski, Igor Mordatch, Karl Pertsch, Kanishka Rao, Krista Reymann, Michael Ryoo, Grecia Salazar, Pannag Sanketi, Pierre Sermanet, Jaspia Singh, Anikait Singh, Radu Soricu, Huong Tran, Vincent Vanhoucke, Quan Vuong, Ayzaan Wahid, Stefan Welker, Paul Wohlhart, Jialin Wu, Fei Xia, Ted Xiao, Peng Xu, Sichun Xu, Tianhe Yu, and Brianna Zitkovich. Rt-2: Vision-language-action models transfer web knowledge to robotic control. In *CoRL*, 2023.

Pieter-Tjerk De Boer, Dirk P. Kroese, Shie Mannor, and Reuven Y. Rubinstein. A Tutorial on the Cross-Entropy Method. *Annals of Operations Research*, 2005.

Peter I. Frazier. A Tutorial on Bayesian Optimization. *arXiv:1807.02811*, 2018.

Rao Fu, Dingxi Zhang, Alex Jiang, Wanjia Fu, Austin Funk, Daniel Ritchie, and Srinath Sridhar. GigaHands: A Massive Annotated Dataset of Bimanual Hand Activities. In *CVPR*, 2025.

Shubham Goel, Georgios Pavlakos, Jathushan Rajasegaran, Angjoo Kanazawa, and Jitendra Malik. Humans in 4D: Reconstructing and Tracking Humans with Transformers. In *ICCV*, 2023.

Félix G. Harvey, Mike Yurick, Derek Nowrouzezahrai, and Christopher Pal. Robust motion in-betweening. In *SIGGRAPH*, 2020.

Tairan He, Zhengyi Luo, Xialin He, Wenli Xiao, Chong Zhang, Weinan Zhang, Kris Kitani, Changliu Liu, and Guanya Shi. OmniH2O: Universal and Dexterous Human-to-Humanoid Whole-Body Teleoperation and Learning. In *CoRL*, 2024.

Tairan He, Jiawei Gao, Wenli Xiao, Yuanhang Zhang, Zi Wang, Jiashun Wang, Zhengyi Luo, Guanqi He, Nikhil Sobanbab, Chaoyi Pan, Zeji Yi, Guannan Qu, Kris Kitani, Jessica Hodgins, Linxi “Jim” Fan, Yuke Zhu, Changliu Liu, and Guanya Shi. ASAP: Aligning Simulation and Real-World Physics for Learning Agile Humanoid Whole-Body Skills. In *RSS*, 2025.

Ryan Hoque, Peide Huang, David J. Yoon, Mouli Sivapurapu, and Jian Zhang. EgoDex: Learning Dexterous Manipulation from Large-Scale Egocentric Video. *arXiv:2505.11709*, 2025.

Taylor Howell, Nimrod Gileadi, Saran Tunyasuvunakool, Kevin Zakka, Tom Erez, and Yuval Tassa. Predictive Sampling: Real-time Behaviour Synthesis with MuJoCo. *arXiv:2212.00541*, 2022.

Zhenyu Jiang, Yuqi Xie, Kevin Lin, Zhenjia Xu, Weikang Wan, Ajay Mandlekar, Linxi Fan, and Yuke Zhu. DexMimicGen: Automated Data Generation for Bimanual Dexterous Manipulation via Imitation Learning. In *ICRA*, 2025.

Jay Kamat, Joaquim Ortiz-Haro, Marc Toussaint, Florian T. Pokorny, and Andreas Orthey. BITKOMO: Combining Sampling and Optimization for Fast Convergence in Optimal Motion Planning. In *IROS*, 2022.

Alexander Khazatsky, Karl Pertsch, Suraj Nair, Ashwin Balakrishna, Sudeep Dasari, Siddharth Karamcheti, Soroush Nasiriany, Mohan Kumar Srirama, Lawrence Yunliang Chen, Kirsty Ellis, Peter David Fagan, Joey Hejna, Masha Itkina, Marion Lepert, Yecheng Jason Ma, Patrick Tree Miller, Jimmy Wu, Suneel Belkhale, Shivin Dass, Huy Ha, Arhan Jain, Abraham Lee, Youngwoon Lee, Marius Memmel, Sungjae Park, Ilija Radosavovic, Kaiyuan Wang, Albert Zhan, Kevin Black, Cheng Chi, Kyle Beltran Hatch, Shan Lin, Jingpei Lu, Jean Mercat, Abdul Rehman, Pannag R Sanketi, Archit Sharma, Cody Simpson, Quan Vuong, Homer Rich Walke, Blake Wulfe, Ted Xiao, Jonathan Heewon Yang, Arefeh Yavary, Tony Z. Zhao, Christopher Agia, Rohan Baijal, Mateo Guaman Castro, Daphne Chen, Qiuyu Chen, Trinity Chung, Jaimyn Drake, Ethan Paul Foster, Jensen Gao, Vitor Guizilini, David Antonio Herrera, Minho Heo, Kyle Hsu, Jiaheng Hu, Muhammad Zubair Irshad, Donovon Jackson, Charlotte Le, Yunshuang Li, Kevin Lin, Roy Lin, Zehan Ma, Abhiram Maddukuri, Suvir Mirchandani, Daniel Morton, Tony Nguyen, Abigail O’Neill, Rosario Scalise, Derick Seale, Victor Son, Stephen Tian, Emi Tran, Andrew E. Wang, Yilin Wu, Annie Xie, Jingyun Yang, Patrick Yin, Yunchu Zhang, Osbert Bastani, Glen Berseth, Jeannette Bohg, Ken Goldberg, Abhinav

Gupta, Abhishek Gupta, Dinesh Jayaraman, Joseph J Lim, Jitendra Malik, Roberto Martín-Martín, Subramanian Ramamoorthy, Dorsa Sadigh, Shuran Song, Jiajun Wu, Michael C. Yip, Yuke Zhu, Thomas Kollar, Sergey Levine, and Chelsea Finn. Droid: A large-scale in-the-wild robot manipulation dataset. In *ICRA*, 2024.

Moo Jin Kim, Karl Pertsch, Siddharth Karamcheti, Ted Xiao, Ashwin Balakrishna, Suraj Nair, Rafael Rafailov, Ethan Foster, Grace Lam, Pannag Sanketi, Quan Vuong, Thomas Kollar, Benjamin Burchfiel, Russ Tedrake, Dorsa Sadigh, Sergey Levine, Percy Liang, and Chelsea Finn. OpenVLA: An Open-Source Vision-Language-Action Model. In *CoRL*, 2024.

Taekyung Kim, Gyuhyun Park, Kiho Kwak, Jihwan Bae, and Wonsuk Lee. Smooth Model Predictive Path Integral Control without Smoothing. *RA-L*, 2022.

Arjun S. Lakshminath, Jessica K. Hodgins, and Nancy S. Pollard. Kinematic Motion Retargeting for Contact-Rich Anthropomorphic Manipulations. *ACM Transactions on Graphics*, 2025.

Albert H. Li, Preston Culbertson, Vince Kurtz, and Aaron D. Ames. DROP: Dexterous Reorientation via Online Planning. In *ICRA*, 2025a.

Jialong Li, Xuxin Cheng, Tianshu Huang, Shiqi Yang, Ri-Zhao Qiu, and Xiaolong Wang. AMO: Adaptive Motion Optimization for Hyper-Dexterous Humanoid Whole-Body Control. In *RSS*, 2025b.

Jiaman Li, Jiajun Wu, and C Karen Liu. Object motion guided human motion synthesis. *ACM Transactions on Graphics*, 2023.

Jinhan Li, Yifeng Zhu, Yuqi Xie, Zhenyu Jiang, Mingyo Seo, Georgios Pavlakos, and Yuke Zhu. OKAMI: Teaching Humanoid Robots Manipulation Skills through Single Video Imitation. In *CoRL*, 2024.

Kailin Li, Puahao Li, Tengyu Liu, Yuyang Li, and Siyuan Huang. ManipTrans: Efficient Dexterous Bimanual Manipulation Transfer via Residual Learning. In *CVPR*, 2025c.

Qiayuan Liao, Takara E Truong, Xiaoyu Huang, Guy Tevet, Koushil Sreenath, and C. Karen Liu. Beyondmimic: From motion tracking to versatile humanoid control via guided diffusion. *arXiv:2508.08241*, 2025.

Vincent Liu, Ademi Adeniji, Haotian Zhan, Siddhant Haldar, Raunaq Bhirangi, Pieter Abbeel, and Lerrel Pinto. EgoZero: Robot Learning from Smart Glasses. *arXiv:2505.20290*, 2025.

Xueyi Liu, Kangbo Lyu, Jieqiong Zhang, Tao Du, and Li Yi. QuasiSim: Parameterized Quasi-Physical Simulators for Dexterous Manipulations Transfer. In *ECCV*, 2024.

Tyler Ga Wei Lum, Olivia Y. Lee, C. Karen Liu, and Jeannette Bohg. Crossing the Human-Robot Embodiment Gap with Sim-to-Real RL using One Human Demonstration. In *CoRL*, 2025.

Naureen Mahmood, Nima Ghorbani, Nikolaus F. Troje, Gerard Pons-Moll, and Michael J. Black. AMASS: Archive of Motion Capture as Surface Shapes. In *ICCV*, 2019.

Zhao Mandi, Yifan Hou, Dieter Fox, Yashraj Narang, Ajay Mandlekar, and Shuran Song. DexMachina: Functional Retargeting for Bimanual Dexterous Manipulation. *arXiv:2505.24853*, 2025.

Ajay Mandlekar, Soroush Nasiriany, Bowen Wen, Iretiayo Akinola, Yashraj Narang, Linxi Fan, Yuke Zhu, and Dieter Fox. Mimicgen: A data generation system for scalable robot learning using human demonstrations. *arXiv:2310.17596*, 2023.

Shie Mannor, Reuven Rubinstein, and Yohai Gat. The Cross Entropy Method for Fast Policy Search. In *ICML*, 2003.

Shinichiro Nakaoka, Atsushi Nakazawa, Fumio Kanehiro, Kenji Kaneko, Mitsuharu Morisawa, and Katsushi Ikeuchi. Task model of lower body motion for a biped humanoid robot to imitate human dances. In *IROS*, 2005.

Chaoyi Pan, Zeji Yi, Guanya Shi, and Guannan Qu. Model-Based Diffusion for Trajectory Optimization. In *NeurIPS*, 2024.

Georgios Papagiannis, Norman Di Palo, Pietro Vitiello, and Edward Johns. R+X: Retrieval and Execution from Everyday Human Videos. In *ICRA*, 2025.

Sungjae Park, Homanga Bharadhwaj, and Shubham Tulsiani. DemoDiffusion: One-Shot Human Imitation using pre-trained Diffusion Policy. *arXiv:2506.20668*, 2025.

Georgios Pavlakos, Dandan Shan, Ilija Radosavovic, Angjoo Kanazawa, David Fouhey, and Jitendra Malik. Reconstructing Hands in 3D with Transformers. In *CVPR*, 2024.

Haozhi Qi, Brent Yi, Sudharshan Suresh, Mike Lambeta, Yi Ma, Roberto Calandra, and Jitendra Malik. General in-hand object rotation with vision and touch. In *CoRL*, 2023.

Yuzhe Qin, Hao Su, and Xiaolong Wang. From One Hand to Multiple Hands: Imitation Learning for Dexterous Manipulation from Single-Camera Teleoperation. In *IROS*, 2022.

Yuzhe Qin, Wei Yang, Binghao Huang, Karl Van Wyk, Hao Su, Xiaolong Wang, Yu-Wei Chao, and Dieter Fox. AnyTeleop: A General Vision-Based Dexterous Robot Arm-Hand Teleoperation System. In *RSS*, 2023.

Delin Qu, Haoming Song, Qizhi Chen, Zhaoqing Chen, Xianqiang Gao, Xinyi Ye, Qi Lv, Modi Shi, Guanghui Ren, Cheng Ruan, Maoqing Yao, Haoran Yang, Jiacheng Bao, Bin Zhao, and Dong Wang. Eo-1: Interleaved vision-text-action pretraining for general robot control. *2508.21112*, 2025.

Daniele Reda, Jungdam Won, Yuting Ye, Michiel van de Panne, and Alexander Winkler. Physics-based Motion Retargeting from Sparse Inputs. *arXiv:2307.01938*, 2023.

Juntao Ren, Priya Sundaresan, Dorsa Sadigh, Sanjiban Choudhury, and Jeannette Bohg. Motion Tracks: A Unified Representation for Human-Robot Transfer in Few-Shot Imitation Learning. *Computer Graphics and Interactive Techniques*, 2025.

Tim Salimans, Jonathan Ho, Xi Chen, Szymon Sidor, and Ilya Sutskever. Evolution Strategies as a Scalable Alternative to Reinforcement Learning. *arXiv:1703.03864*, 2017.

John Schulman, Filip Wolski, Prafulla Dhariwal, Alec Radford, and Oleg Klimov. Proximal policy optimization algorithms. *1707.06347*, 2017.

Kenneth Shaw, Shikhar Bahl, and Deepak Pathak. VideoDex: Learning Dexterity from Internet Videos. In *CoRL*, 2022.

Zilin Si, Jose Enrique Chen, M. Emre Karagozler, Antonia Bronars, Jonathan Hutchinson, Thomas Lampe, Nimrod Gileadi, Taylor Howell, Stefano Saliceti, Lukasz Barczyk, Ilan Olivarez Correa, Tom Erez, Mohit Shridhar, Murilo Fernandes Martins, Konstantinos Bousmalis, Nicolas Heess, Francesco Nori, and Maria Bauza. Exostart: Efficient learning for dexterous manipulation with sensorized exoskeleton demonstrations. 2025. URL <https://arxiv.org/abs/2506.11775>.

RDT Team. Rdt2: Enabling zero-shot cross-embodiment generalization by scaling up umi data, 2025. URL <https://github.com/thu-ml/RDT2>.

Josh Tobin, Rachel Fong, Alex Ray, Jonas Schneider, Wojciech Zaremba, and Pieter Abbeel. Domain Randomization for Transferring Deep Neural Networks from Simulation to the Real World. In *IROS*, 2017.

Chen Wang, Linxi Fan, Jiankai Sun, Ruohan Zhang, Li Fei-Fei, Danfei Xu, Yuke Zhu, and Anima Anandkumar. MimicPlay: Long-Horizon Imitation Learning by Watching Human Play. In *CoRL*, 2023.

Bowen Wen, Wei Yang, Jan Kautz, and Stan Birchfield. FoundationPose: Unified 6D Pose Estimation and Tracking of Novel Objects. In *CVPR*, 2024.

Haoyang Weng, Yitang Li, Nikhil Sobanbabu, Zihan Wang, Zhengyi Luo, Tairan He, Deva Ramanan, and Guanya Shi. HDMI: Learning interactive humanoid whole-body control from human videos. *arXiv:2509.16757*, 2025.

Grady Williams, Paul Drews, Brian Goldfain, James M. Rehg, and Evangelos A. Theodorou. Aggressive driving with model predictive path integral control. In *ICRA*, 2016.

Grady Williams, Brian Goldfain, Paul Drews, Kamil Saigol, James Rehg, and Evangelos Theodorou. Robust Sampling Based Model Predictive Control with Sparse Objective Information. In *RSS*, 2018.

Albert Wu, Ruocheng Wang, Sirui Chen, Clemens Eppner, and C. Karen Liu. One-Shot Transfer of Long-Horizon Extrinsic Manipulation Through Contact Retargeting. *arXiv:2404.07468*, 2024.

Jianfeng Xiang, Zelong Lv, Sicheng Xu, Yu Deng, Ruicheng Wang, Bowen Zhang, Dong Chen, Xin Tong, and Jiaolong Yang. Structured 3D Latents for Scalable and Versatile 3D Generation. In *CVPR*, 2025.

Mengda Xu, Han Zhang, Yifan Hou, Zhenjia Xu, Linxi Fan, Manuela Veloso, and Shuran Song. DexUMI: Using Human Hand as the Universal Manipulation Interface for Dexterous Manipulation. In *CoRL*, 2025.

Haoru Xue, Chaoyi Pan, Zeji Yi, Guannan Qu, and Guanya Shi. Full-Order Sampling-Based MPC for Torque-Level Locomotion Control via Diffusion-Style Annealing. In *ICRA*, 2025.

Lujie Yang, Xiaoyu Huang, Zhen Wu, Angjoo Kanazawa, Pieter Abbeel, Carmelo Sferrazza, C Karen Liu, Rocky Duan, and Guanya Shi. Omnidretarget: Interaction-preserving data generation for humanoid whole-body loco-manipulation and scene interaction. *arXiv:2509.26633*, 2025a.

Lujie Yang, H. J. Terry Suh, Tong Zhao, Bernhard Paus Graesdal, Tarik Kelestemur, Jiuguang Wang, Tao Pang, and Russ Tedrake. Physics-Driven Data Generation for Contact-Rich Manipulation via Trajectory Optimization. In *RSS*, 2025b.

Zhao-Heng Yin, Changhao Wang, Luis Pineda, Krishna Bodduluri, Tingfan Wu, Pieter Abbeel, and Mustafa Mukadam. Geometric Retargeting: A Principled, Ultrafast Neural Hand Retargeting Algorithm. In *IROS*, 2025a.

Zhao-Heng Yin, Changhao Wang, Luis Pineda, Francois Hogan, Krishna Bodduluri, Akash Sharma, Patrick Lancaster, Ishita Prasad, Mrinal Kalakrishnan, Jitendra Malik, Mike Lambeta, Tingfan Wu, Pieter Abbeel, and Mustafa Mukadam. DexterityGen: Foundation Controller for Unprecedented Dexterity. In *RSS*, 2025b.

Yanjie Ze, Zixuan Chen, João Pedro Araújo, Zi-ang Cao, Xue Bin Peng, Jiajun Wu, and C. Karen Liu. TWIST: Teleoperated Whole-Body Imitation System. In *CoRL*, 2025.

Xinyu Zhan, Lixin Yang, Yifei Zhao, Kangrui Mao, Hanlin Xu, Zenan Lin, Kailin Li, and Cewu Lu. OAKINK2: A Dataset of Bimanual Hands-Object Manipulation in Complex Task Completion. In *CVPR*, 2024.

Han Zhang, Songbo Hu, Zhecheng Yuan, and Huazhe Xu. DOGlove: Dexterous Manipulation with a Low-Cost Open-Source Haptic Force Feedback Glove. In *RSS*, 2025.

Yifan Zhong, Xuchuan Huang, Ruochong Li, Ceyao Zhang, Zhang Chen, Tianrui Guan, Fanlian Zeng, Ka Num Lui, Yuyao Ye, Yitao Liang, Yaodong Yang, and Yuanpei Chen. DexGraspVLA: A Vision-Language-Action Framework Towards General Dexterous Grasping. *arXiv:2502.20900*, 2025.

# Appendix

## A Implementation Details

### A.1 Preprocessing

We extract a 21D keypoint representation per hand using 3D fingertip positions and 6D wrist pose from MANO. An IK solver maps these keypoints to robot-specific joint positions by minimizing  $\mathcal{L}_{\text{IK}} = \sum_{i=1}^n \|\mathbf{p}_i^{\text{robot}} - \mathbf{p}_i^{\text{human}}\|^2 + 0.1 \|\mathbf{R}_{\text{wrist}}^{\text{robot}} - \mathbf{R}_{\text{wrist}}^{\text{human}}\|_F^2$ . Trajectories are resampled at 50 Hz and low-pass filtered at 10 Hz.

### A.2 Hyperparameters and Setup

All experiments use: horizon  $H = 1.2$  s, particles  $N = 1024$ , temperatures  $\beta_1 = 0.85, \beta_2 = 0.9$ , iterations  $M = 16$ , and annealing  $\eta_t = \eta_0 \cdot 1.1^t$  with  $\eta_0 = 0.01$ . Each experiment is repeated 5 times with different seeds. The method supports multiple simulators: MuJoCo Warp, MJX, Genesis, and Isaac Gym. All simulations run at 100 Hz physics and 50 Hz control in MuJoCo Warp (most datasets) and Genesis (ARCTIC dataset, as in DexMachina (Mandi et al., 2025)). Ablations and speed tests use RTX 4090 GPUs; dataset generation uses H100 GPUs.

### A.3 Retargeting for RL Policy Training

This section describes the training details for the RL policy in section 4.2. We use the PPO algorithm Schulman et al. (2017) and port implementation from Weng et al. (2025).

**Rewards.** We use the following rewards:

- Body tracking reward: tracking humanoid pelvis, hand and legs body motion.
- Object tracking reward: tracking the object motion.
- Action rate penalty: penalize the action rate to avoid jittering.

We remove the contact reward, self-collision penalty as well as the auxiliary contact reward proposed in the paper to evaluate the reference motion retargeting quality.

**Termination.** We terminate the training when the average body tracking error is greater than 10 cm and the average object tracking error is greater than 10 cm.